

THE EFFECT OF ACID MODIFICATION ON ADSORPTION OF ORTHO-NITROPHENOL FROM AQUEOUS SOLUTION BY MULTI WALL CARBON NANOTUBES AND CONICAL CARBON NANOFIBERS: CHARACTERIZATION, MODELLING AND PERFORMANCE

HAMZA A. ASMALY¹, NASSERELDEEN KABBASHI^{1*},
MA'AN FAHMI AL-KHATIB¹, MD ZAHANGIR ALAM¹, ADAM SULAMAN²

¹*Department of Chemical Engineering and Sustainability, International Islamic University Malaysia, Gombak, 53100 Kuala Lumpur, Malaysia.*

²*Core Research Facilities Center, King Fahd University for Petroleum and Minerals, Dhahran, Saudi Arabia*

**Corresponding authors: nasreldin@iium.edu.my*

ABSTRACT: This study examined the absorption of ortho-nitrophenol onto Conical carbon nanofibers (CCNFs) and multi-wall carbon nanotubes (MCNTs). The properties of the CNTs and CNFs were analyzed using various techniques such as X-ray diffraction, scanning electron microscopy, Fourier-transform infrared spectroscopy, Brunauer-Emmett-Teller for surface area analysis, Energy dispersive X-ray spectroscopy and transmission electron microscopy. The study investigated the effectiveness of hydrochloric acid-activated the surface of both CNTs and CNFs in removing 2-NitroPhenol ions from an aqueous solution. The Central-Composite design of RSM was employed to study the impact of solution pH, agitation speed, adsorption time, and adsorbent dosage on the adsorption process and then optimize these parameters for the removal of 2NP. The results of the optimization revealed that the best conditions for removing 2-Nitro Phenol were pH 6.6, for 68.0 minutes, at 80 rpm agitation and 108mg of adsorbent. Additionally, the effect of the initial concentration was evaluated, and the adsorption capacity of the nano-activated carbon adsorbents was calculated. The study found that multi-wall carbon nanotubes (MWCNTs) with a high surface area are more effective than Conical carbon nanofibers (CCNFs) in reducing 2-NP from an aqueous solution, making MWCNTs a potentially useful material in the fight against environmental pollution.

KEY WORDS: *2-Nitrophenol, Conical Carbon nanofibers, Multiwall Carbon nanotubes, Adsorption.*

1. INTRODUCTION

Water bodies and wastewater often contain phenolic compounds, which can be found in the petroleum and petrochemical industries, as well as in the coal conversion and phenol production sectors [1]. The chemical, insecticide, and pharmaceutical industries rely heavily on NPs as a primary raw material. It has been used in a variety of manufacturing processes, from the creation of medications (such acetaminophen and aspirin) through the creation of synthetic colors, explosives, pharmaceuticals, and the darkening of leather [2]. The risks

that many phenols cause to human health and other forms of life have led to their listing as hazardous pollutants. Particularly, 2-NP which has been classified as a priority contaminant due to its high concentrations in the environment and the lack of attention it has received from researchers around the world [3]. The USEPA states that NP's maximum containment values range from 0.01-2.0 g/L [4]. Health consequences of high concentration than (2.0g/L) of 2-NP including cyanosis, cataracts, dermatitis, headaches, drowsiness, nausea, and eye irritation [5,6]. Scholars confirmed that Methemoglobin can be formed in the human body when 2-NP reacts with blood-borne hemoglobin. This causes blood disorders and reduces red blood cells' capacity to carry oxygen to tissues and other organs [7]. Considering this, the removal of these NP molecules has emerged as a top priority contaminant, with the goal of protecting both the environment and the health of humans [8,9].

There are several approaches for purifying water from NPs products that have been identified in the literature [10,11], but Due to the low cost and efficiency in a variety options, adsorption has been found to be one of the best methods for removing these pollutants and reducing concentrations in the effluents at very low levels [12,13,14]. Adsorbents of several types, including active carbon, clay ore, chelating substances, natural chitosan/zeolites, etc., have been developed [15,16,17,18]. During the past two decades, nanotechnology has received a lot more attention than it did before. The use of carbon nanomaterials for water purification is widely recognized as effective. Fullerenes, carbon nanotubes, graphene, and carbon nanofibers all have the potential to be used in the purification of wastewater [19,20]. Nanoparticles have an excellent potential for participation in water purification. Its exclusive features, such as high surfaces, mechanical properties, increased chemical reactivity and lower costs enable the precise removal from the water of toxic metallic ions, viruses, bacteria, organic and inorganic solutes. In Fact, the carbon nanostructures have high porosity and hollow structures, which have a massive surface to volume ratio. Furthermore, carbon nanomaterials have high availability of various functionalities and are easier to chemically modify, practically carbon nano tubes and carbon nanofibers [21].

CNTs have been the subject of numerous studies since its discovery by Iijima, Sumio in 1991, according to the amazing physicochemical properties they demonstrate [22]. The earliest CNTs discovered (MWCNTs), consisted of up to several tens of graphitic shells separated by 0.34 nm, with diameters of 1 nm and a considerable length/diameter ratio [23]. MWCNTs can be thought of as elongated fullerenes [24]. Ebbesen and Ajayan [25] released their work on the bulk synthesis of MWCNTs by arcing graphite electrodes in inert atmospheres under optimal current and pressure settings a few months after Iijima's discovery. CNTs are interesting carbon-based adsorptive materials and new adsorbents for several reasons. They have a higher specific surface area than activated carbons and are superior in chemical inertness during physical adsorption. Contrary to activated carbon, CNTs have a more uniform atomic structure. CNTs have clearly defined adsorption sites that may be employed immediately, whereas activated carbons require measurement of their pore diameter distribution and adsorption energy distribution to evaluate adsorption. In terms of CNT architecture, both single crystal and polycrystalline carbonaceous adsorptive materials are virtually identical [26]. The excellent adsorption properties of the CNTs encourage researchers to use them as an effective adsorbent. CNTs treated with nitric acid were shown to be more selective in their adsorption of lead and copper from water, as reported by Li et al. [35]. At the optimal pH 6.8, he discovered that the maximal adsorption

capabilities for Pb^{2+} and Cu^{2+} were 97.08 mg/g and 24.49 mg/g, respectively. Functionalized SWCNT was utilized as an adsorbent by Deng et al. [36] to extract Pb^{2+} from water. It was determined that at a pH of 5.0, it has an adsorption capacity of 406.6 mg/g. Within 40 minutes, the process had stabilized at its equilibrium state. In addition, organic dyes (methylene blue) were eliminated by MWCNTs, as demonstrated by the work of Shaolin et al. [37]. At the optimal pH6, he found that 59.7 mg/g of methylene blue could be absorbed. It is suggested that the adsorption process be prolonged or alternative methods be used to circumvent the limitations of these investigations.

On the other hand, CNFs are the second novel member of the carbon family, and their distinctive chemical, physical, mechanical, and electrical characteristics make them promising materials for a wide range of technical applications [27,28]. CNFs normally have diameters ranging from 50 to 200 nm, whereas carbon nanotubes often have sizes smaller than 100 nm, according to Shaffer study on the diameter variation of fibrous graphitic materials [29]. CNF may be synthesized using catalysts and carbon sources. Laser ablation vaporizes a few catalysts and initiates CNF growth just in front of the graphite target (generally transition metals). Hydrocarbons (carbon sources) are deposited at temperatures between 500 and 1200°C on metal catalysts (Fe, Co, and Ni) using the Chemical Vapor Depositing Approach [30]. It has been shown that carbon nanofiber may be used to adsorb hazardous compounds from water by both Park et al. [31] and Kim et al. [32]. Compared to other nanomaterials, carbon nanofibers were superior at selectively absorbing alcohol from water. Also, Lee et al. [33] used carbon nanofibers to detoxify arsenic in discarded materials. He found that arsenic's highest adsorption capacity was 0.18 mg/g at the optimal pH5. In about 5 hours, equilibrium was reached in this procedure. Even after 5 hours of processing, his arsenic adsorption capability was poor. Chakraborty et al. used carbon nanofibers to eliminate phenol and lead in water more effectively. The equilibration times for phenol and lead were 12 and 36 hours, respectively. Phenol and lead adsorb 275 and 35 mg/g, respectively, at optimum pH 6.8. Despite having a high adsorption capacity, the method takes far too long. To solve such limitations, this study proposed high-speed adsorption [34].

This study examines the effectiveness of using Conical Carbon Nanofiber (CCNF) and Multi-walled Carbon Nanotube (MCNT) in removing 2-NP from water via surface activation with hydrochloric acid. The optimal adsorption conditions were studied, and the removal efficiency was compared.

2. MATERIALS AND METHODS

2.1 Materials

The Conical Carbon Nanofibers used in this research were supplied by the Chinese company Hebei Liche Zhuoge Environmental Technology Co., Ltd. The CCNFs were found to be 99.99% pure, with a diameter of 75-25 nm and a length of 20-30 μm . The Multi-Walled Carbon Nanotubes (MWCNTs) used in this experiment were purchased from Sigma Aldrich. with less than 2000 ppm for trace metals. They had an average diameter of 8.7 nm, an outer diameter of 6.0 nm, a length of 2.5-20 m and an inner diameter of 2.0 nm, and a purity of 98.99%.

2.2 Methods

2.2.1 Surface Activation of the CCNFs and MCNTs Adsorbents

In this step, the received CCNFs and MCNTs were treated with 35% hydrochloric acid, which is a well-established technique for impurity elimination. 3 moles of 200 ml were achieved using a dilution of 50 ml of HCl. Then in a 500 ml Erlenmeyer flask, one gram of CCNFs/MCNTs was deposited, and 200 ml of HCl was added. The mixture was stirred for 3 hours with a magnetic stirrer, then the CCNF and MCNTs were separated from their solution using a centrifuge (Sigma model 3-16KL) at 4500 min⁻¹ speed for 15 minutes at 21°C, filtered, and rinsed four times with deionized water to neutral pH. Then it was vacuum dried at 40°C overnight.

2.2.2 Preparation of the stock solution

A stock solution of 2-Nitro Phenol (from Sigma Aldrich) with initial concentration of 5 ppm was prepared by serial dilution of 1000 ppm solution made from dissolved 1000 mg of 2-NP (powder) in 1.0 L deionized water generated by using ELGA instrument model LA 759. 1.0 M nitric acid (HNO₃) and 1.0 M sodium hydroxide (NaOH) were used to adjust the pH of the stock solution. Throughout the experiment, buffer solutions were used to keep the pH constant.

2.2.3 Batch adsorption experiment

At room temperature, batch adsorption studies were carried out to determine the efficiency of 2-NP adsorption by activated CCNFs and MCNTs. The impact of the initial 2-NP concentration (2 to 15 PPM) was examined through batch test. The impact of the other parameter including the contact time (10–360 min), agitation speed (50-250) rpm (5– 7), and adsorbent dosage (10–300 g/L) were obtained from the RSM method after optimization the parameters by using Experimental design V13. The experiment were conducted in 100 ml volumetric flasks, and the 2-NP concentrations were determined by measuring the maximum absorbance wave lengths of 279 nm using a Uv - visible spectrophotometer Eq (1), with the adsorption capacity calculated by Eq(2) as follows:

$$\% \text{ Removal} = \left(\frac{C_i - C_e}{C_i} \right) 100 \quad (1)$$

$$Q = \left(\frac{C_i - C_e}{M_{\text{adsorbent}}} \right) * V_{\text{sol}} \quad (2)$$

where Q is the adsorption capacity (mg/g), C_i is the initial concentration of 2-NP solution (mg/L), C_e is the equilibrium 2-NP concentration (mg/L), V_{sol} is the total volume of 2-NP solution (L) and M_{adsorbent} (g) is the CCNFs and MCNTs mass, respectively.

2.2.4 Characterization Techniques

The crystallinity of the CCNFs and MCNTs was evaluated by X-ray diffraction (XRD) with a Rigaku diffractometer (Miniflex II), under the conditions of Cu K α radiation analysis ($\lambda = 1.5405\text{\AA}$) with an electricity source of 30 kV and 15 mA, a step size of 0.03°

and a count period of 0.5 s per step. The CNFs and CNTs was coated with gold material by using Quorum instrument model (Q150TE), then images from High-Resolution Scanning Electron Microscope (SEM) (Czech Republic) were taken and EDX was also performed. Also, The JEOL 2100 transmission electron microscope (TEM) was utilized to analyze the morphological and structural properties of the original and the activated CNF and CNTs. The surface area was calculated at 77°K using nitrogen adsorption/desorption isotherms obtained with a model NOVA 3200e automated gas sorption system (Quanta chrome, USA). Each sample was degassed for 6 hours at 150 degrees Celsius prior to measurement. The Brunauer-Emmett-Teller (BET) equation was used to calculate the specific surface area [38]. The KBr disc technique was used to perform FT-IR spectrophotometric analysis on a Nicolet model FT-IR 6700 (USA).

2.2.5 Analysis of Response Surface Method (RSM)

Response Surface Methodology (RSM) is a set of mathematical and statistical tools used to design experiments, build models, evaluate the effects of operating conditions, and identify the optimal values of factors to achieve a target response. In this study, RSM was applied to determine the optimal conditions for the adsorption of 2-NP from water by conducting experiments within the range of each factor. RSM was also used to refine models after identifying the significant factors that impact 2-NP removal, including pH, adsorption time, agitation speed, and dosage. The Central-Composite method of RSM was utilized to obtain the optimum parameters for removal of 2-NP and these were employed in the experiments of this study.

2.2.6 Adsorption-based Central Composite Design (CCD)

Table 1 displays the codec factors and corresponding values for the adsorption parameters used by the RSM. Analysis of variance (ANOVA) was used to analyze the data in Design Expert Version 13. (Stat Ease, USA). The design included 30 experiments with 16 factorial points (2 duplicates), 4 central points (4 replicates), and 8 axial points (2 replicates) with a 95% confidence interval.

Table 1: Experimental design for removal of 2-NP by CNT and CNF

	Name	Units	Low	High	-alpha	+alpha
A [Numeric]	pH		5.5	7	4.75	7.75
B [Numeric]	Adsorption Time	min	10	360	-165	535
C [Numeric]	Agitation Speed	rpm	50	250	-50	350
D [Numeric]	Adsorbent Dosage	mg	10	300	-135	445

3. RESULTS AND DISCUSSION

3.1 Adsorbents Characterization

3.1.1 Energy Dispersive X-ray

EDX analyses were used to identify the elements present on the surface CCNFs and MCNTs after they were activated with HCL. Figures 1(a) and 1(b) displayed electron images of the samples, revealing a difference in surface structure between the two types of nano carbon. These findings were consistent with the spectrum images in Figure 1. The attached table in figure 1 shows the Elemental analysis of Modified Adsorbents (wt %). It was noted that the CCNFs had a higher percentage of carbon present, followed by trace amounts of impurities such as Rb, Si and Al. In contrast, the CCNFs had a high percentage of carbon covering its surface with no impurities present. The high weight percentage of the Carbon in the pure Activated MCNTs was found 96.4 compared with 100 in the pure CCNFs. The high percentage of carbon in the nano carbon adsorbents samples is expected to lead to high performance in adsorption of the 2-NP.

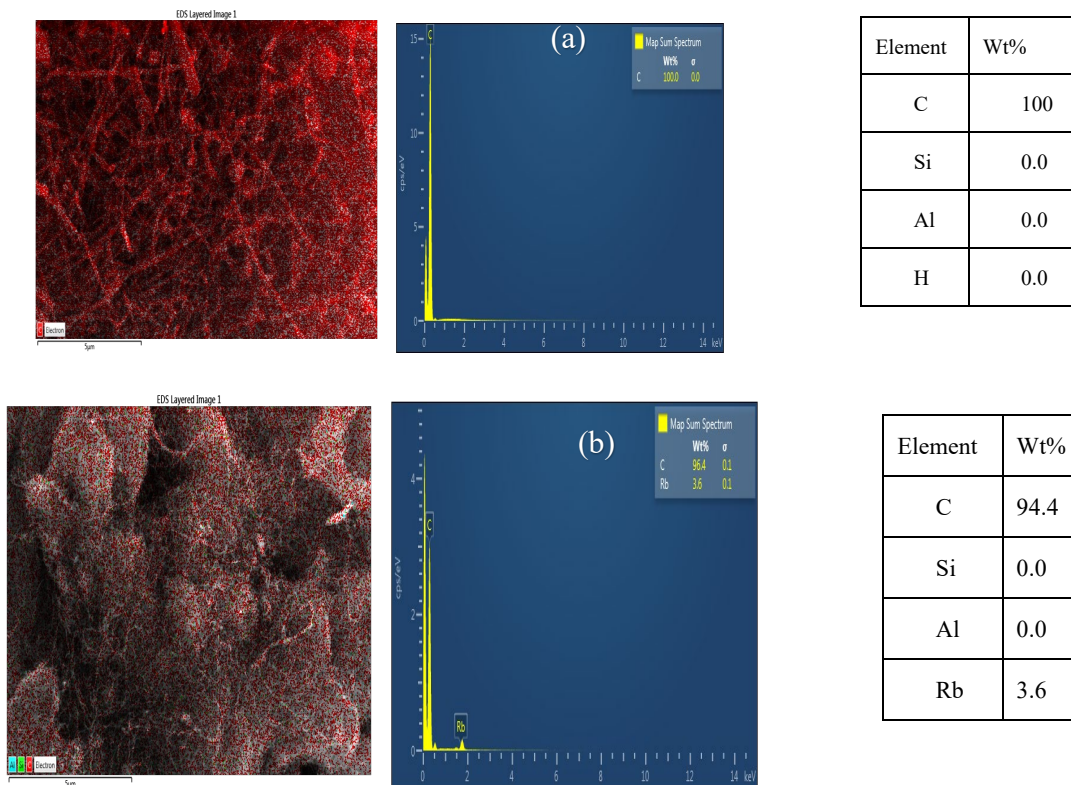


Fig. 1. EDX spectrums of the (a)CNFs and (b)CNTs.

3.1.2 Brunauer–Emmett–Teller (BET) Surface Area Analysis

As indicated in Table 2, the isotherms were utilized to compute the BET area, Langmuir area, total pore volume, and pore size of the adsorbents before and after activation with Hydrochloric acid. As shown in Fig. 2 a-b, the BET surface area values obtained for CNFs and CNF/HCL were 24.559 and 58.334 m²/g, respectively. The surface area of Langmuir was determined to be 66.393 and 230.359 m²/g. Furthermore, the estimated surface area of

the CNFs and CNF/HCL using DFT technique rose dramatically from 24.10 to 54.45 m²/g. The increase in CNF surface area caused by the three techniques indicates that more adsorption sites are available because of nanoparticle activation at the CNF surface. The BET surface area of the CNTs and CNTs/HCL was found to be 184.18 and 221.34 m²/g, respectively, as shown in Fig. 2 c-d. While the Langmuir surface area was found 707.774 and 1205.043 m²/g. According to Density Functional Theory (DFT) calculations, the total surface area of CNFs and CNF/HCL significantly increased from 24.1 to 54.45 m²/g. Activation of the CNF surface by nanoparticles results in a rise in available adsorption sites, as evidenced by the CNF's increased surface area.

The pore volume and pore size of a nano adsorbents sample are determined using techniques such as the Horvath-Kawazoe (HK) method, the Saito-Foley (SF) method, and the Density Functional Theory method, as seen in table 2. Following CNF activation and evaluation using the HK and SF techniques, the pore volume drastically increased, going from 3.875x10⁻³ to 1.866x10⁻² (cm³/g) and from 5.82x10⁻³ to 1.1512x10² (cm³/g), respectively. The DFT approach found that the volume of the CNFs grew from 2.367x10⁻² to 7.66x10⁻² (cm³/g) because of the activation procedure. This finding is comparable to how the activation process impacted the surface of the CNFs. The pore volume of the activated CNTs samples rose by 7.6x10⁻², 6.1x10⁻² and 2.7 x10⁻¹ to 1.1x10⁻¹, 8.6x10⁻², and 8.11x10⁻¹, respectively, when the HK, SF, and DFT were used.

Table 2: Surface area analysis of the raw and Activated adsorbents with HCL.

Sample	S _{BET} (m ² /g)	S _{Langmuir} (m ² /g)	S _{DFT} (m ² /g)	Pore Volume (cc/g)			Pore Size (Å)		
				HK	SF	DFT	HK	SF	DFT
Raw/CNF	24.559	66.393	24.1	3.875*10 ⁻³	5.82*10 ⁻³	2.3671*10 ⁻²	8.537	19.1	5.305
Activated/CNF	58.334	230.359	54.45	1.866*10 ⁻²	1.512*10 ⁻²	7.662*10 ⁻²	3.862	8.443	8.900
Raw/CNT	184.18	707.774	188.8	7.648*10 ⁻²	6.134*10 ⁻²	2.748*10 ⁻¹	1.838	2.261	5.305
Activated/CNT	221.34	1205.043	259.32	1.1*10 ⁻¹	8.6*10 ⁻²	8.11*10 ⁻¹	3.213	5.537	3.925

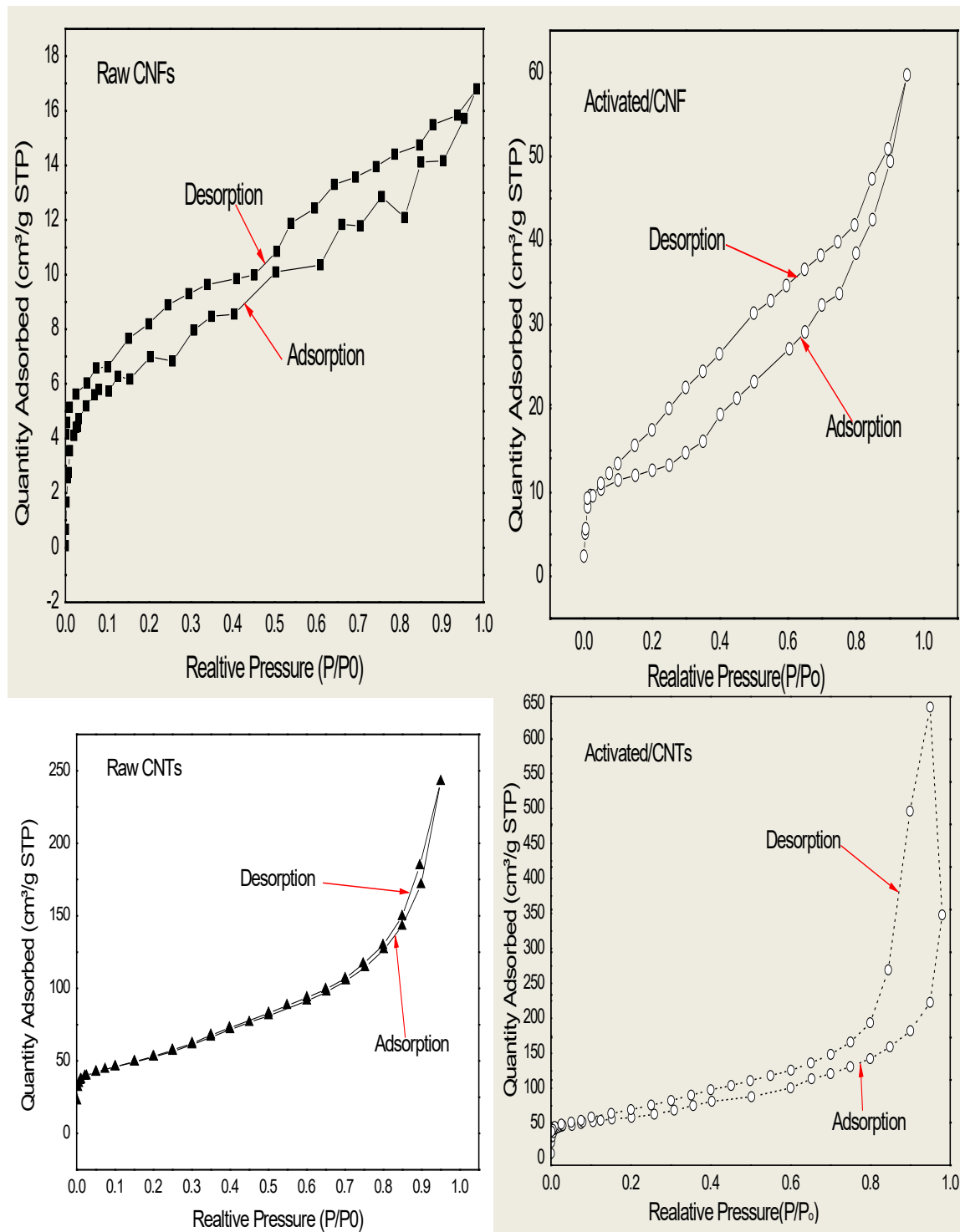


Fig. 2. Surface area measurements of raw and treated CNFs and CNTs with HCl.

The Horvath-Kawazoe (HK) method is used to understand the adsorption and diffusion characteristics of activated Nano Carbon adsorbents, as shown in Figure 3, which shows the change in pore size for activated CNTs and active CNFs. The volume holes of MCNTs are more sensitive to the activation process than those of CNFs, as seen in the figure, resulting in a more granular distribution of volume pores in CNTs compared to CNFs. The Fig also

demonstrated that the two adsorbents possessed Type IV nitrogen isotherms (ESI), indicating that the CNTs and CNFs were mostly microporous.

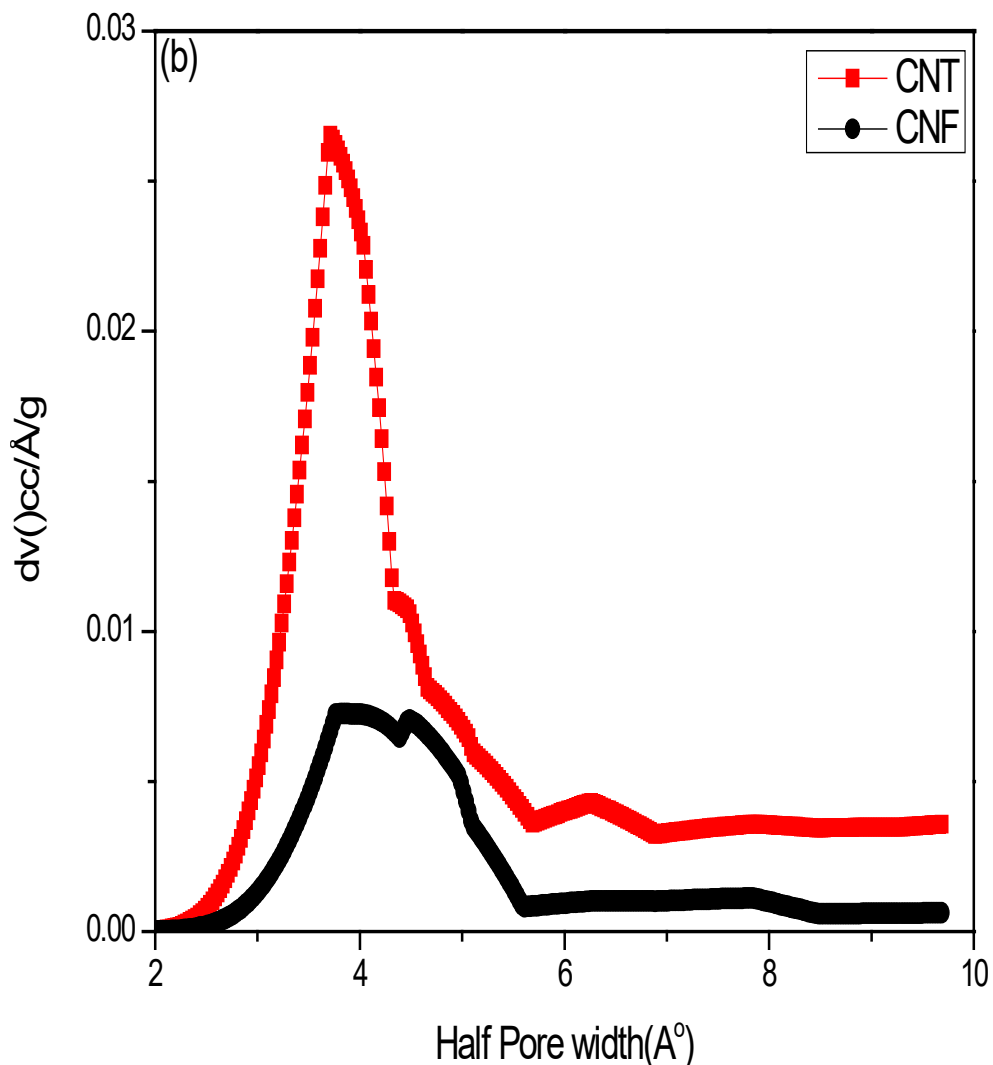


Fig. 3. Effective Pore volume and pore size distributions of the treated CNF and MCNT calculated by Horvath-Kawazoe method.

3.1.3 FTIR Spectroscopy

The FT-IR technique, which is widely used to analyze chemical structure changes, is considered a crucial characterization method.” The surface chemistry of CNF and CNT adsorbents that were both activated and inactivated were evaluated through FTIR. The FTIR spectra of original and treated CNFs and CNTs were seen in Figure 4(a and b). The C=C stretching vibrations are represented by the bands of CNFs (Figure 4a) spectra at 1630 cm^{-1} . The C-O stretching represented by the spectra at 11051 cm^{-1} , while the band at 3430 cm^{-1} corresponds to the vibration of the O-H groups. The C-H bending vibrations in CNTs are indicated by a band at around 1386 cm^{-1} in Figure b. This band is a result of the bending vibrations of the C-H group in the graphene rings, which are caused by the C=C stretching and bending vibrations of the graphene structure. The broad band in the range of $3200\text{--}3550$

cm^{-1} in Figure 4b is related to the vibrations of the O–H groups. A weak band at 1717 cm^{-1} is associated with the stretching of the C=O bond [41].

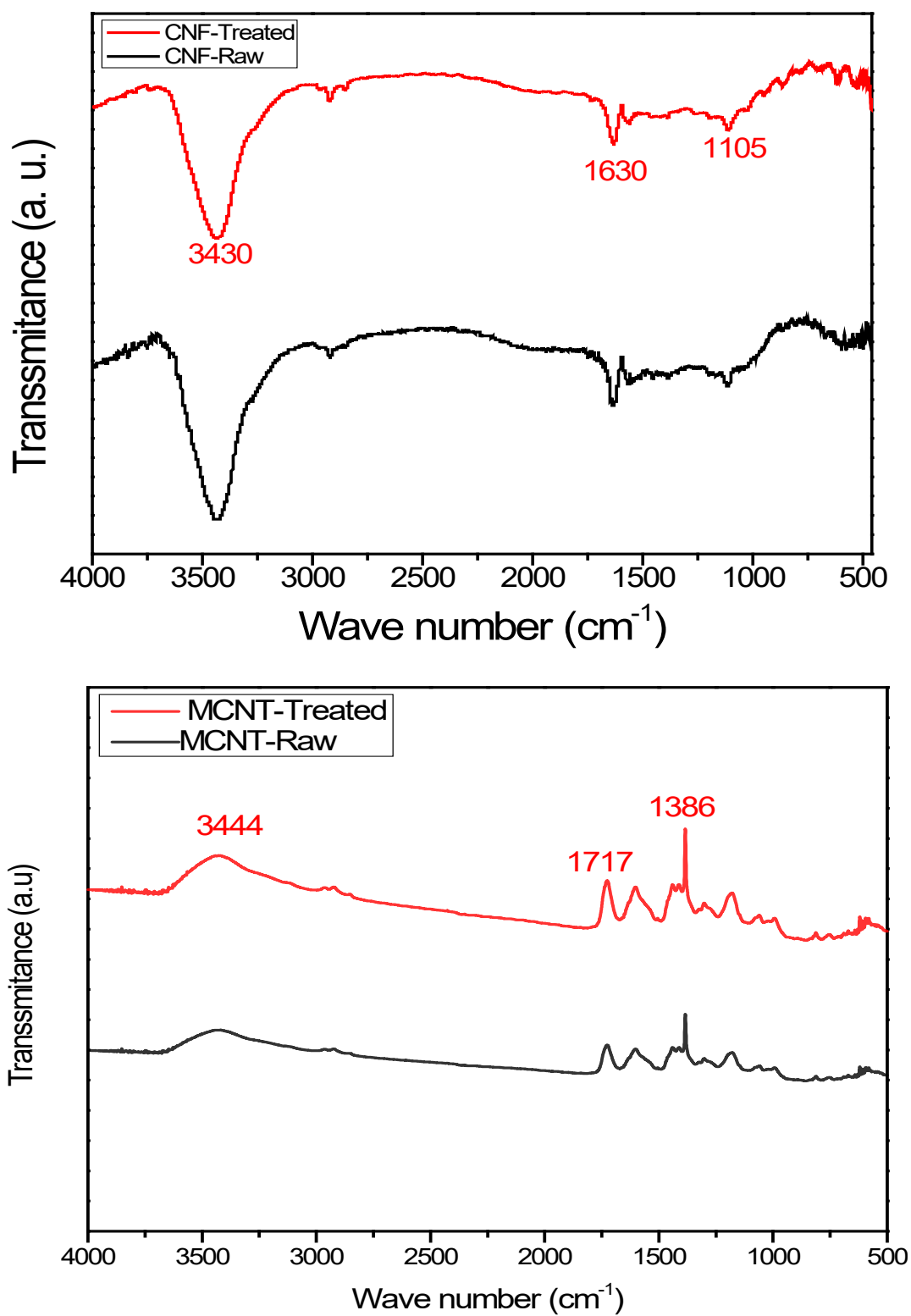


Fig. 4. Spectra of the received and treated with HCL for CNFs and CNTs.

3.1.4 X-Ray Diffraction (XRD) for CNF and CNTs

As can be observed in Figure 5a and 5b, the crystal structures of CNFs and CNTs, which are used as nano carbon adsorbents, have been validated using XRD analysis. Only two different size peaks are seen for CNFs, with angles of 26.6° and 44.7° degrees respectively. These angles correspond to the (002) and (101) planes of hexagonal graphite crystallites. This crystalline structure was found to be consistent with the findings of earlier studies conducted by other authors [42]. CNTs, on the other hand, display one large and the other is a small peak at around 25° and 44° , which correspond to the (002) and (101) facets of graphitic carbon. These peaks are clearly shown in the graph below. The great purity of the CNFs and CNTs, as shown by EDX analysis in Fig (1), along with the impact of having their surfaces activated by HCL may cause the peaks of these two types of nanostructures to disappear.

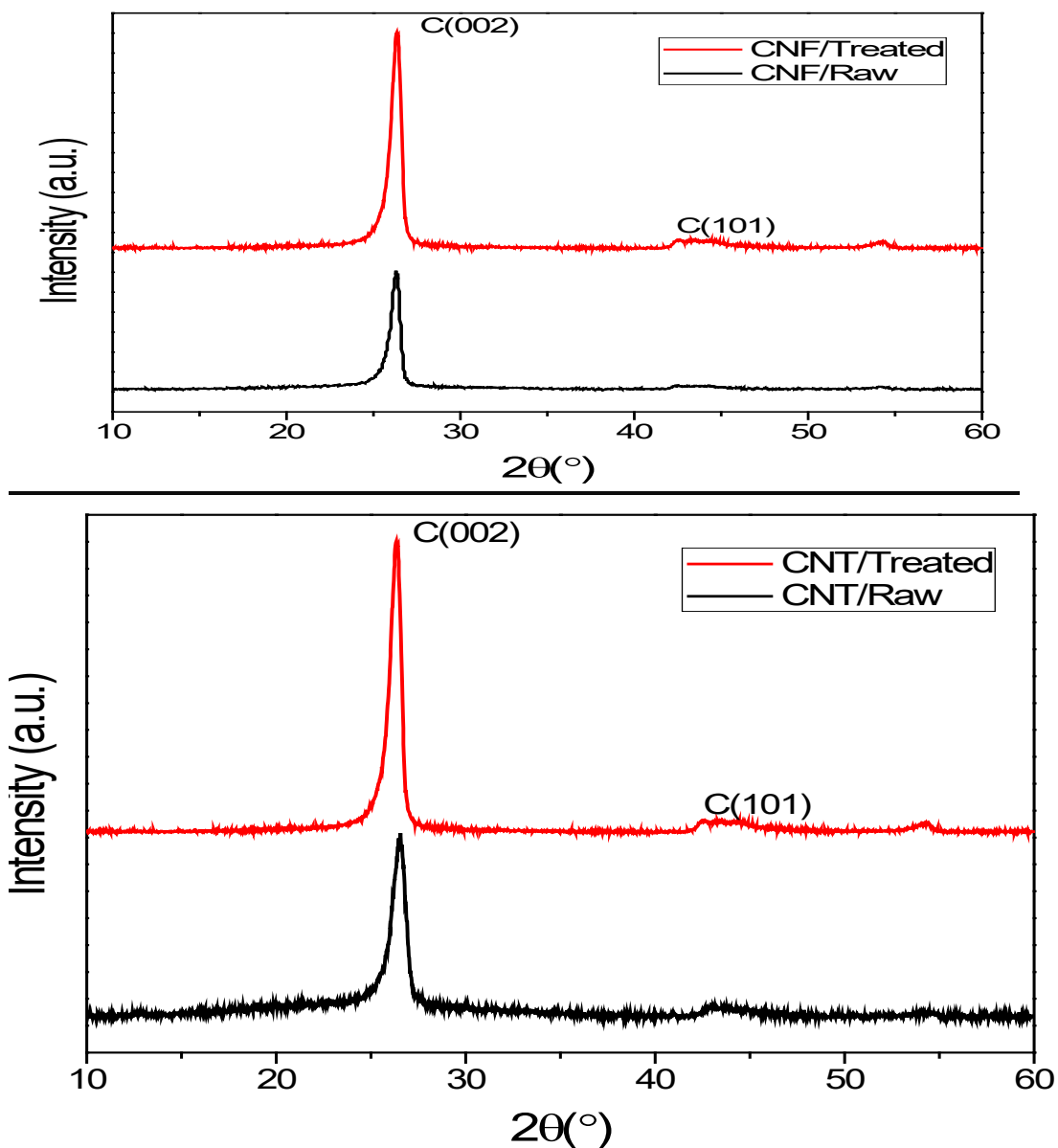
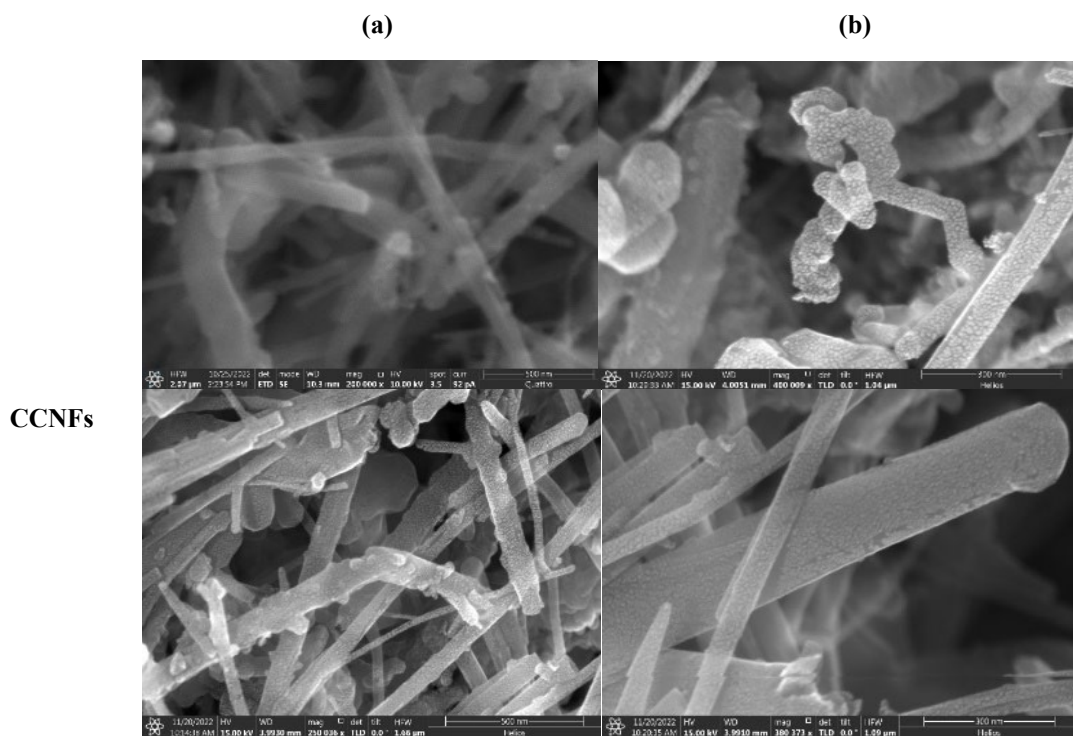


Fig. 5. XRD of the received and treated of CNFs and CNTs.

3.1.5 Morphology and Microstructure of CNFs and CNTs

The shape and microstructure of CNFs and CNTs before and after surface modification were exhibited in microphotographs (Fig 6). The SEM images indicated that the sample contained Nanofibers of various sizes and lengths with an average diameter of 78.15nm. Morphological analysis utilizing SEM images indicated no significant differences between raw CNFs (Figure 5(a)) and CNFs activated by HCL (Figure 5(a)). The fibrous architecture of randomly distributed threads tangled together was preserved in these CNFs. SEM analysis of the product showed that the CNTs were entangled with one another and had a cylindrical shape with an average diameter of 14.53 nm (Figure 6). (c). Photos (Figure 6(d)) showed that when the CNT was treated with HCL, the resulting substrates had a very different, more transparent morphology than the raw CNTs' surfaces. This is evident when compared to the surface morphology of CNTs (Figure 6c). Images captured by the SEM don't appear to reveal the typical tubular shapes of CNTs, but rather a uniform layer covering their surfaces.



MCNTs

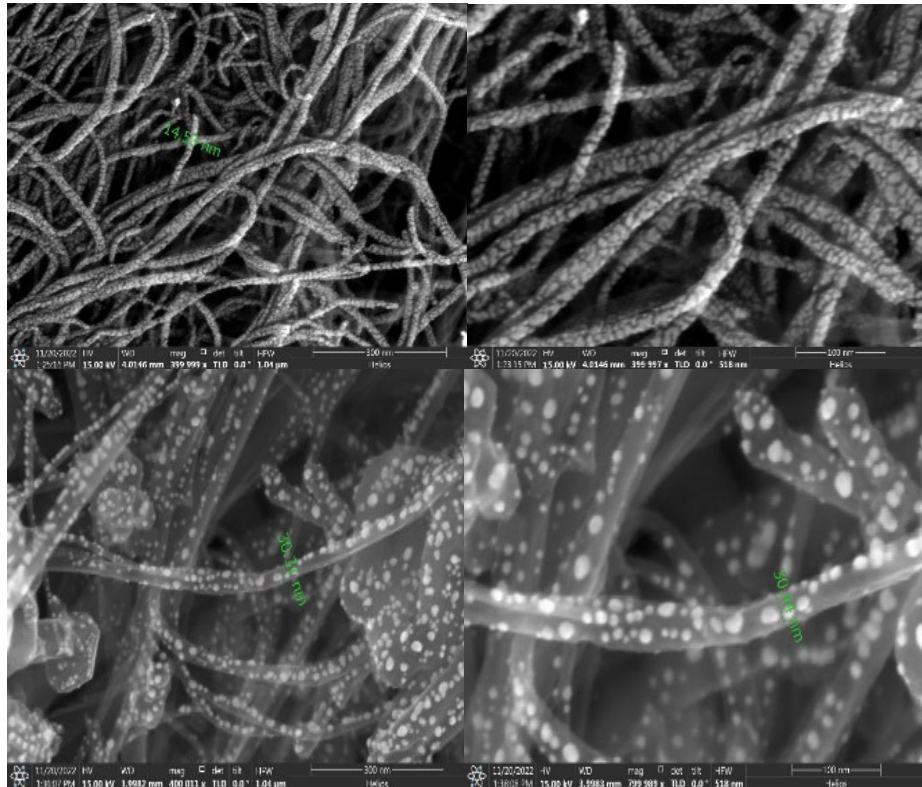


Fig. 6. SEM images at different Magnification for the CNFs and CNTs (a) as received (b) Treated by HCL.

3.1.6 Transmission Electron Microscopy (TEM)

Figure 7 displays TEM micrographs of both CNFs and CNTs in their two phases (original and activated). The diameters of the achieved nanofibers overlap with the SEM image. At the nanoscale, the photos show their characteristic spiral helix shape. The CNF structure is seen as a continuous cone-helix, with the presence of pyrolytic amorphous carbon also visible. The morphology and stability of nanofibers and nanotubes are critical because they enable greater removal efficiency via adsorption of 2-NP molecules in solution. As shown in Figure 7, since the structure of the tubes in CNTs is more regular than that of the fibers in CNFs, we anticipate that the nanotubes will have a better performance than the nanofibers when it comes to the removal of 2-NP irons from aqueous solutions.

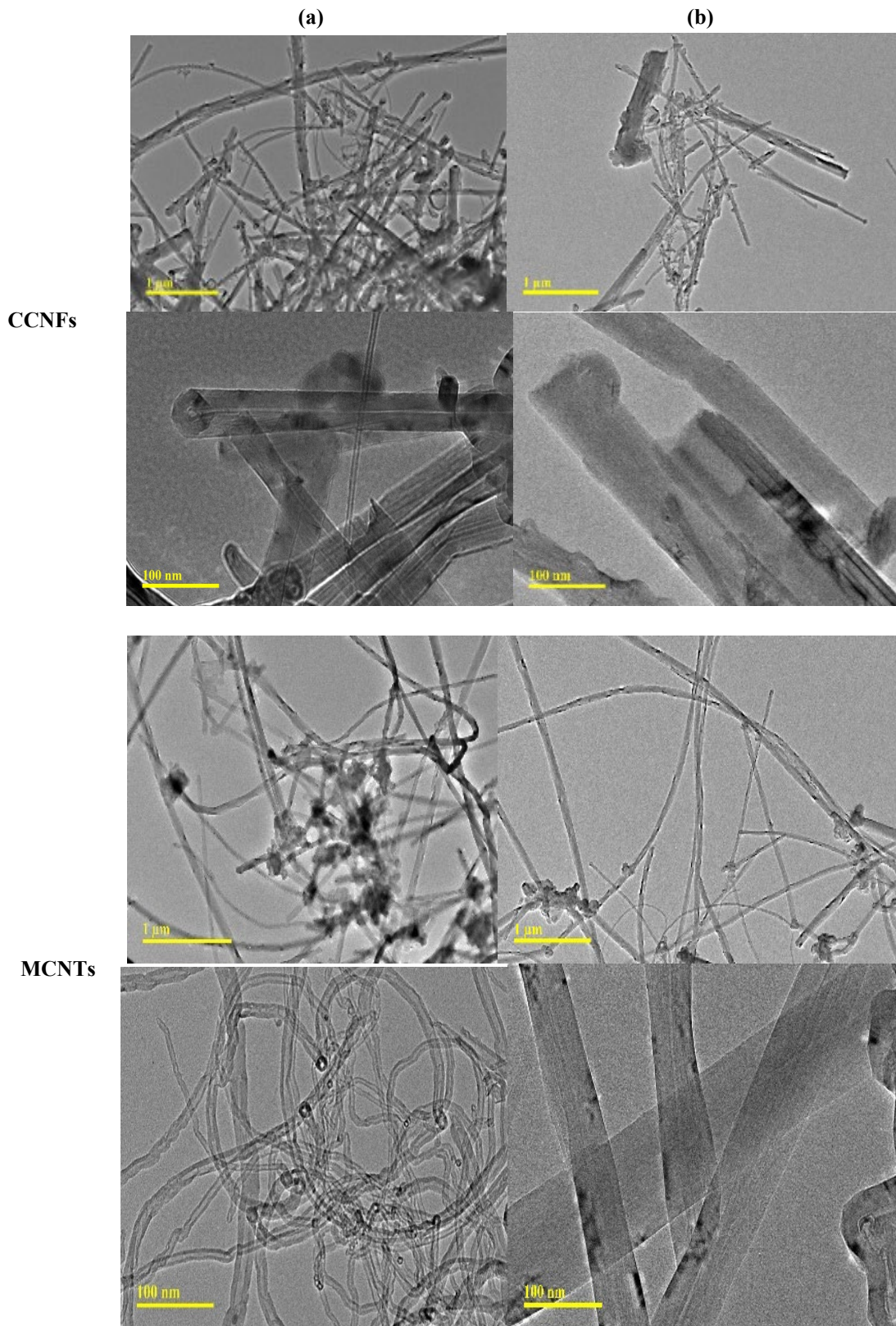
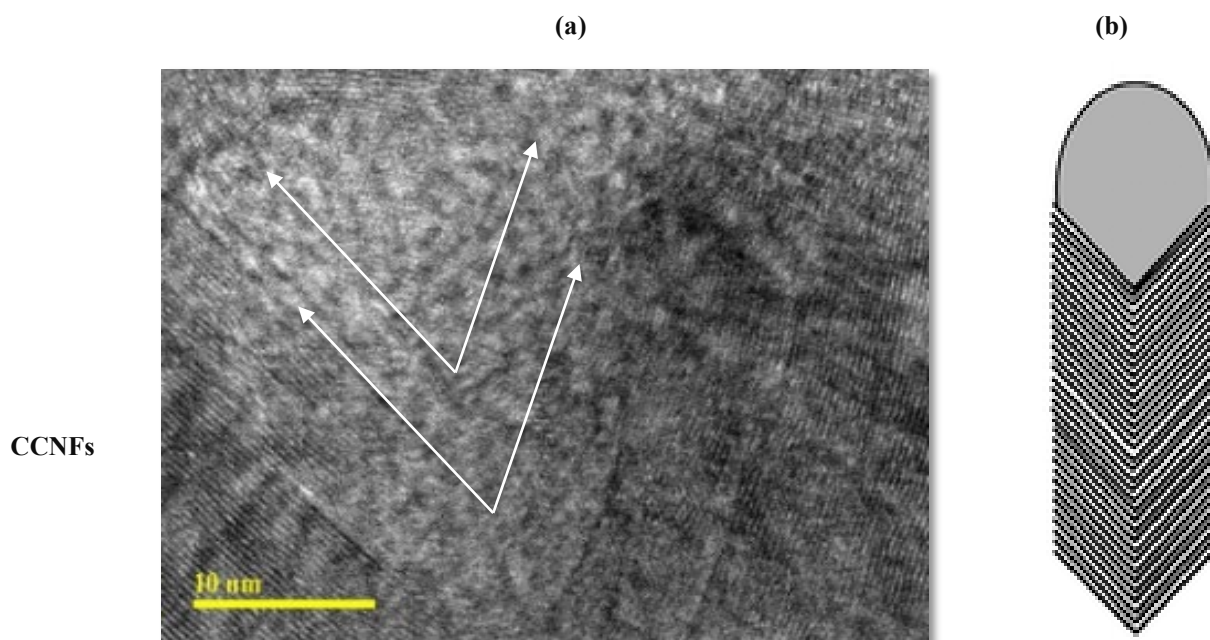


Fig. 7. TEM images at different Magnifications for the CNFs and CNTs (a) as received(b,) Treated by HCL.

The images in figure (8) also showed the stiffness of the graphitic carbon structure. The layered CNF structure was clearly visible in the high-resolution image, as indicated by the brown Lines. The image revealed that the CNF microstructures contained both herringbone and more graphitic conically, which was in line with previous research findings [43,44,45]. In the TEM image, the structure of the carbon nanotubes can be observed as parallel lines, which are the layers of graphene rolled up. The high-quality image highlights the layered structure of the CNTs, as seen in the white arrows. The distance between the lines indicates the diameter of the CNT. The image of figure 8 (a) shows that the CNTs are of different diameters and lengths, as well as defects in the structure.



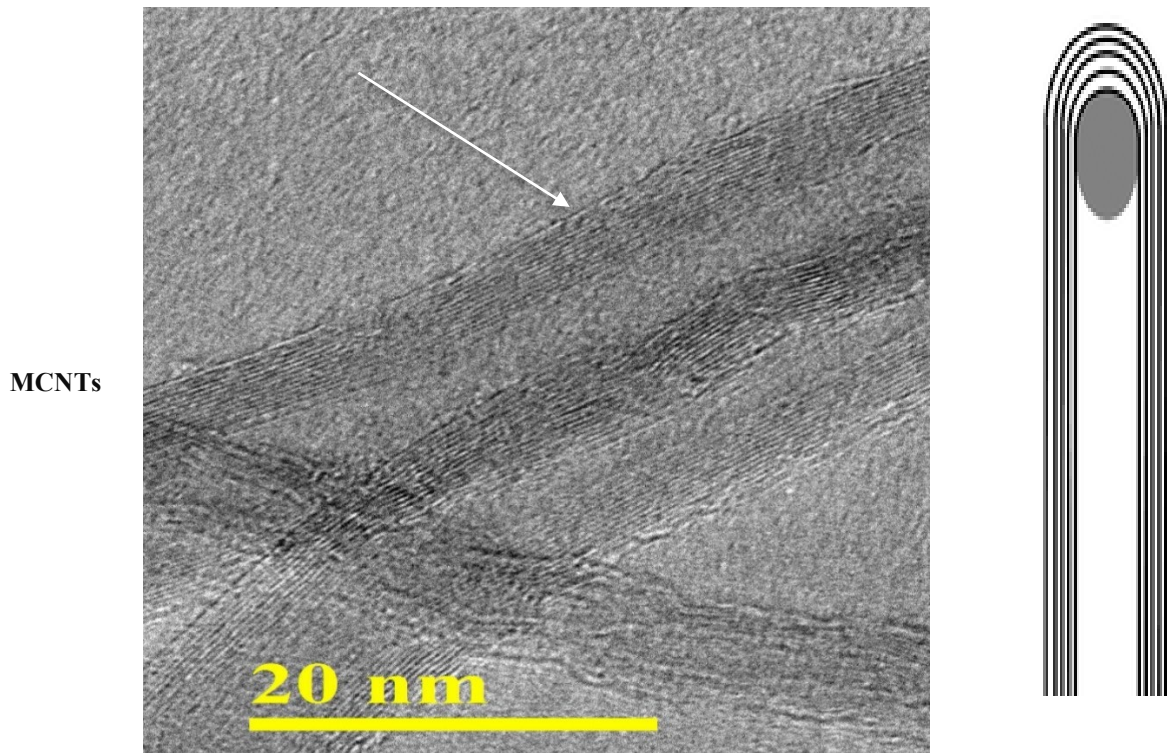


Fig. 8. Graphitic structure of CCNFs and MCNTs (a) TEM images of this study (b) As reported in literature by Philippe [50]).

3.1.7 Response Surface Method (RSM) Analysis Results

In this investigation, two levels and four factors were referred to as "k," and the total number of runs was determined by the formula 2^k . In Table 1, the parameters that need to be optimized are listed, along with the values for each level. In Table 3, on the other hand, the actual experimental conditions that were used for each of the 50 runs are listed. The results of fifty separate experiments are summarized in Table 3, which demonstrates how successfully CNTs were able to extract 2-NP from water.

Figure 9 illustrates the correlation between the actual and predicted parameters, as well as the normal probability versus the residual, together with the deviation from the reference point in relation to the removal of 2-NP. Additionally, this figure presents an illustration of the deviation from the reference point in relation to the removal of 2-NP.

Table 3: Experimental design results for 2-NP removal

		Factor 1	Factor 2	Factor 3	Factor 4	Response 1
Std	Run	A: pH %	B: Time hr	C: Speed rpm	D: Dossage mg	Removal %
20	1	6	175	150	155	41.9
12	2	7	120	50	300	69.93
26	3	6	65	150	155	76.37
21	4	6	65	50	155	94
24	5	6	65	150	445	83.9
13	6	5	10	250	300	86.09
25	7	6	65	150	155	82.33
7	8	5	120	250	10	79.88
15	9	5	120	250	300	64.28
8	10	7	120	250	10	80.2
1	11	5	10	50	10	97
28	12	6	65	150	155	79.1
10	13	7	10	50	300	95
3	14	5	120	50	10	73.22
9	15	5	10	50	300	97
11	16	5	120	50	300	72.41
16	17	7	120	250	300	67.46
6	18	7	10	250	10	77.4
4	19	7	120	50	10	77.98
2	20	7	10	50	10	96
27	21	6	65	150	155	83.94
17	22	4	65	150	155	96
30	23	6	65	150	155	82.69
18	24	8	65	150	155	88
5	25	5	10	250	10	79.8
22	26	6	65	350	155	65.37
14	27	7	10	250	300	83.63
23	28	6	65	150	135	83.78
19	29	6	-45	150	155	77.04
29	30	6	65	150	155	88.14

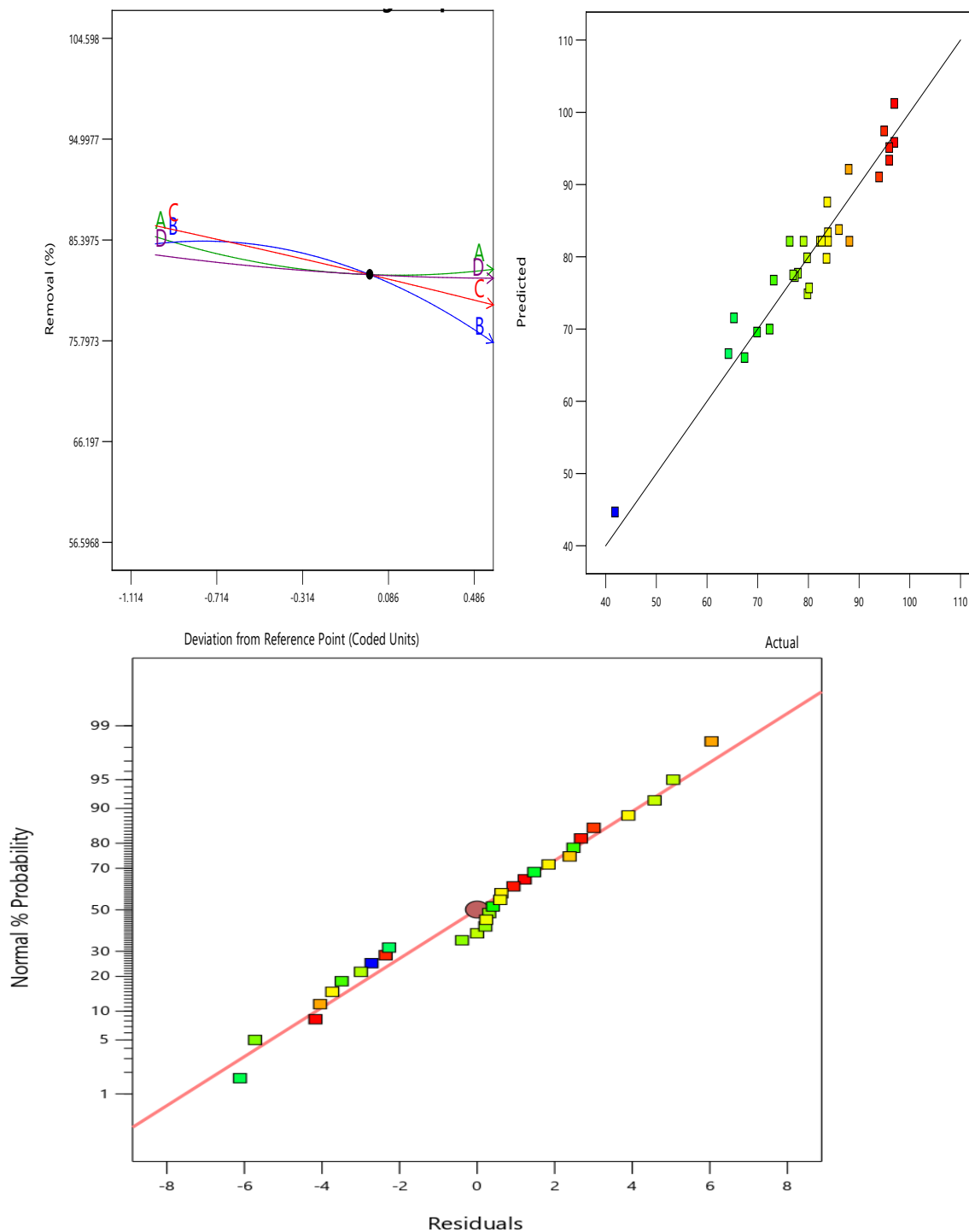


Fig. 9. Plot for 2-NP Removal (a) Perturbation (b) Predicted Vs Actual (c) Normal Plot for Residuals.

The effect of the interaction of pH, duration, speed, and dosage on the removal of 2-NP is shown in Figure 10.

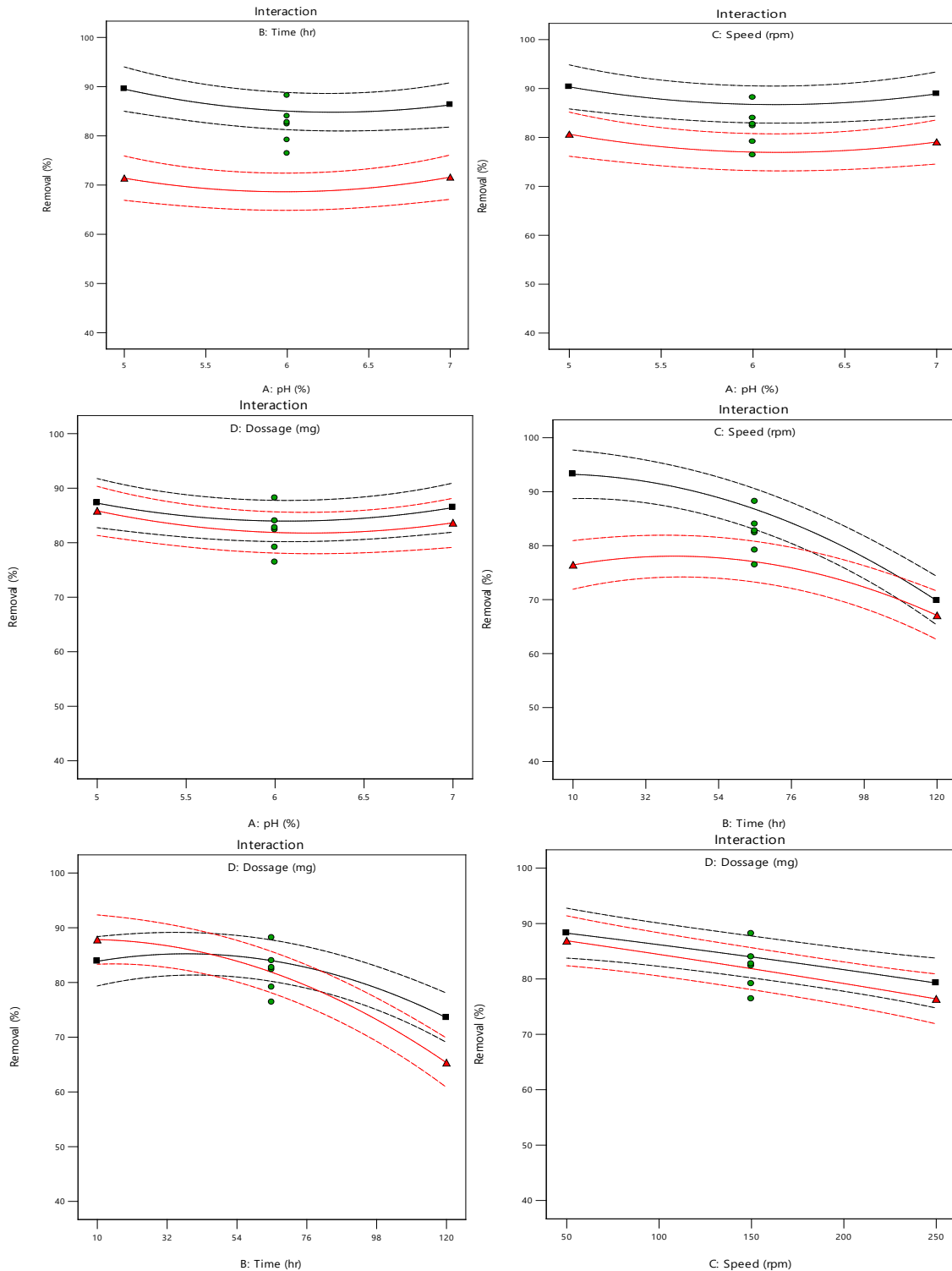


Fig. 10. Plots interaction of the parameters (Ph, time, speed, and Dosage) for 2-NP Removal.

The plots of adsorption time (in hours) and agitation speed (in rpm) and their influence on the removal of 2-NP are shown as a response surface plot as well as a contour plot in Figure 11.

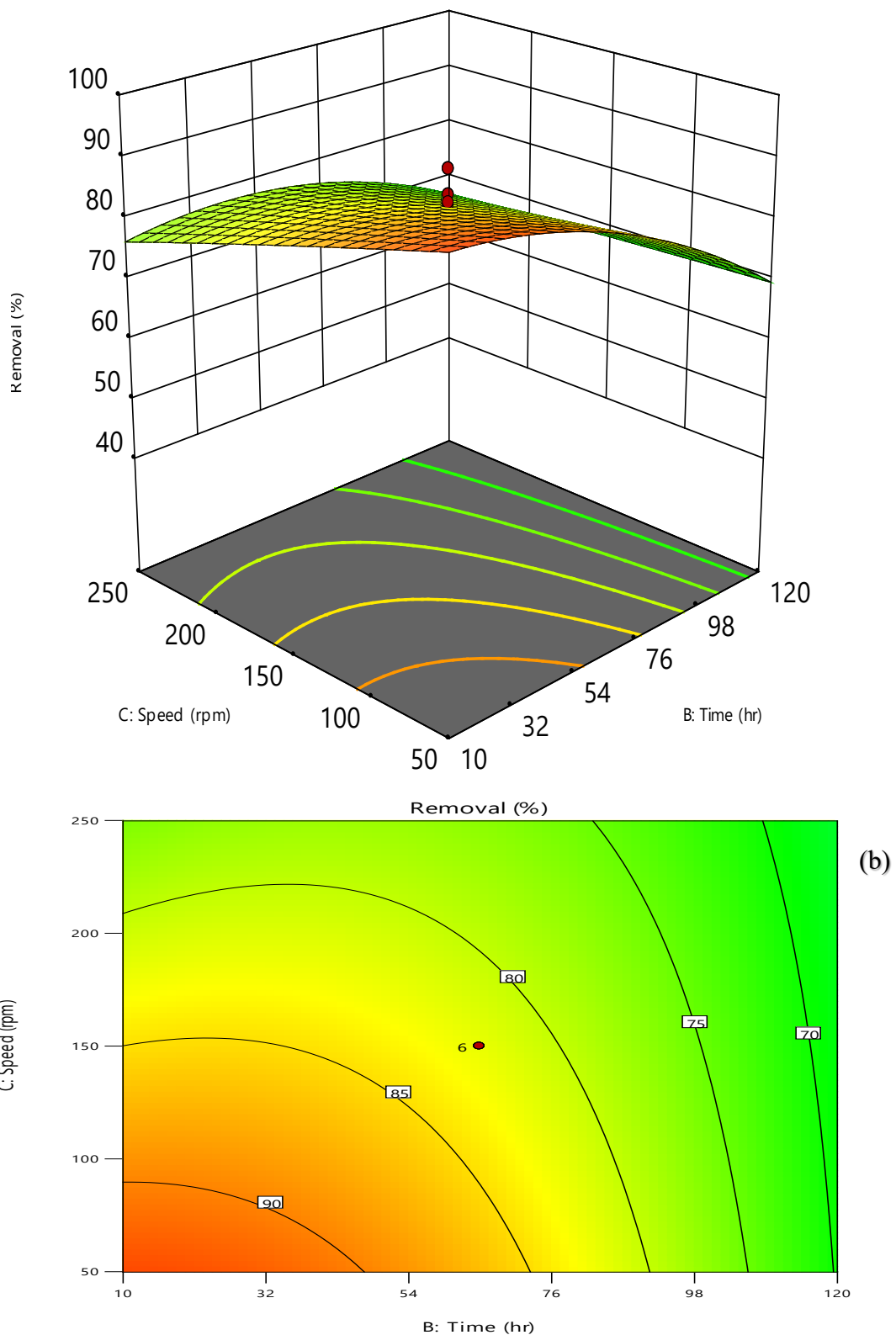


Fig. 11. Plot of adsorption time(hr) and the agitation speed(rpm) on the removal of 2-NP: (a) Response surface plot and (b) Contour plot.

3.1.8 ANOVA Analysis

Table 3's results were analyzed using the ANOVA approach, and Table 4 shows the model's ANOVA response. revealing that the Model F-value of 13.74 indicates that the model is significant for 2-NP removal efficiency with an F-value this big might arise owing to pure error just 0.01% of the time. Model terms with P-values less than 0.0500 are significant. The B, C, BC, BD, A², B² are crucial model terms in this situation. Values larger than 0.1000 imply that the model terms are insignificant. The Lack of Fit F-value of 1.28 indicates that the Lack of Fit is insignificant in comparison to the pure error. A significant Lack of Fit F-value owing to error has a 41.37% probability of occurring. A non-significant lack of fit is desirable.

Table 4: ANOVA results of the Quadric model of 2-NP adsorption using CNT.

Source	Sum of Squares	df	Mean Square	F-value	p-value	
Model	3752.11	14	268.01	13.74	< 0.0001	significant
A-pH	13.62	1	13.62	0.6981	0.4165	
B-Time	1614.42	1	1614.42	82.74	< 0.0001	
C-Speed	570.96	1	570.96	29.26	< 0.0001	
D-Dosage	26.97	1	26.97	1.38	0.2581	
AB	11.63	1	11.63	0.5960	0.4521	
AC	0.0256	1	0.0256	0.0013	0.9716	
AD	1.85	1	1.85	0.0948	0.7624	
BC	198.53	1	198.53	10.18	0.0061	
BD	148.35	1	148.35	7.60	0.0147	
CD	2.22	1	2.22	0.1138	0.7405	
A ²	225.11	1	225.11	11.54	0.0040	
B ²	761.11	1	761.11	39.01	< 0.0001	
C ²	1.26	1	1.26	0.0644	0.8032	
D ²	18.66	1	18.66	0.9563	0.3436	
Residual	292.66	15	19.51			
Lack of Fit	210.56	10	21.06	1.28	0.4137	not significant
Pure Error	82.10	5	16.42			
Cor Total	4044.77	29				

Table 5 displays the model's fit statistics. The R² score of 0.9276 is more than 0.90, indicating that the model is significant. Furthermore, the discrepancy between the Predicted R² of 0.6709 and the Adjusted R² of 0.8601 is less than 0.2. The signal-to-noise ratio is measured by Adeq Precision. A ratio larger than 4 is preferred. The ratio of 18.104 suggests that the signal is acceptable. This model is useful for navigating design space.

Table 5: fit statistics.

Std.Dev.	4.42	R²	0.9276
Mean	80.66	Adjusted R²	0.8601
C.V. %	5.48	Predicted R²	0.6709
		Adeq Precision	18.1045

3.1.9 Optimization of the Parameter using RSM

Table 6 presents the parameter values that were used in the RSM method of optimization.

Table 6: Constraints.

Name	Goal	Lower Limit	Upper Limit	Lower Weight	Upper Weight	Importance
A:pH	is in range	5.5	7	1	1	3
B:Time	is in range	30	150	1	1	3
C:Speed	maximize	50	250	1	1	3
D:Dossage	is in range	10	300	1	1	3
Removal	none	41.9	97	1	1	5

Table 7 shows the outcomes of that method of optimization of the adsorption of 2-NP

Table 7: Expermental result of the optimization(50Runs)

Number	pH	Time	Speed	Dosage	Removal	Desirability
1	6.493	44.429	166.685	144.757	83.565	1.000
2	7.000	120.000	250.000	300.000	65.988	1.000
3	7.000	120.000	250.000	10.000	75.623	1.000
4	7.000	120.000	50.000	10.000	77.668	1.000
5	7.000	120.000	50.000	300.000	69.523	1.000
6	6.441	106.194	123.411	107.636	75.284	1.000
7	5.623	97.565	161.492	27.917	78.638	1.000
8	6.407	105.925	196.959	152.880	72.441	1.000
9	6.352	79.889	231.618	94.132	77.418	1.000
10	5.904	131.388	148.024	45.513	68.548	1.000
11	6.609	141.869	187.037	250.295	58.286	1.000
12	5.642	115.404	155.037	134.835	70.967	1.000
13	6.076	134.100	168.044	91.466	65.767	1.000
14	6.474	118.709	195.924	212.620	67.425	1.000
15	6.117	123.771	236.600	140.783	66.711	1.000
16	6.346	40.662	153.724	222.689	84.657	1.000
17	5.867	68.098	188.804	74.605	80.907	1.000

18	6.515	141.883	102.791	27.629	66.567	1.000	
19	6.948	136.084	138.222	65.491	69.211	1.000	
20	5.999	69.906	221.156	235.548	77.334	1.000	
21	6.264	86.503	188.698	69.665	78.529	1.000	
22	6.109	112.745	236.078	290.372	66.237	1.000	
23	6.822	58.282	99.201	272.366	86.816	1.000	
24	5.772	33.060	214.328	101.434	80.889	1.000	
25	5.756	77.202	184.043	295.993	77.959	1.000	
26	6.694	99.850	246.748	256.021	71.129	1.000	
27	6.008	99.657	248.525	246.278	70.226	1.000	
28	6.731	122.915	156.399	52.719	72.787	1.000	
29	6.704	121.072	140.315	283.386	66.664	1.000	
30	5.827	103.033	207.393	125.143	73.270	1.000	
31	6.842	81.604	104.765	26.927	84.946	1.000	
32	5.981	47.980	213.837	150.520	80.265	1.000	
33	5.872	147.214	166.322	71.019	61.641	1.000	
34	6.726	63.233	179.726	172.658	81.636	1.000	
35	5.622	106.785	158.806	103.228	74.354	1.000	
36	6.673	134.196	198.800	291.337	60.414	1.000	
37	6.868	132.036	137.813	239.427	64.108	1.000	
38	6.648	67.537	79.608	107.991	87.138	1.000	Selected
39	6.751	63.136	240.387	198.822	78.283	1.000	
40	6.687	119.671	60.581	174.402	70.721	1.000	
41	5.807	55.962	130.583	295.703	84.997	1.000	
42	6.979	90.794	203.546	235.171	76.262	1.000	
43	5.797	129.448	84.373	288.243	62.446	1.000	
44	6.929	144.238	111.804	108.861	64.040	1.000	
45	6.358	30.456	111.179	202.397	88.174	1.000	
46	6.843	123.443	131.016	98.519	71.695	1.000	
47	5.612	74.044	65.359	51.547	85.958	1.000	
48	6.323	71.234	246.423	47.188	78.504	1.000	
49	5.727	119.156	214.348	297.926	64.770	1.000	
50	6.881	128.379	151.368	161.182	67.855	1.000	

Thorough some consideration of these parameters values, the decision was made to focus on the specific solution (Run #38) that yielded the highest percentage of removal for 2-NP. It was found that maintaining a pH of 6.6 resulted in a Prediction removal rate of 87.13%. if the amount of adsorbents used was 108 grams and the agitation speed was set at 80 rounds per minute for the duration of the 1 hour and 7 minute for all adsorption process. Figure 12 showed the graphical optimum parameter for adsorption 2-NP by CNTs. These parameters for Optimization result in run (38) was confirmed and used it in the experimental study.

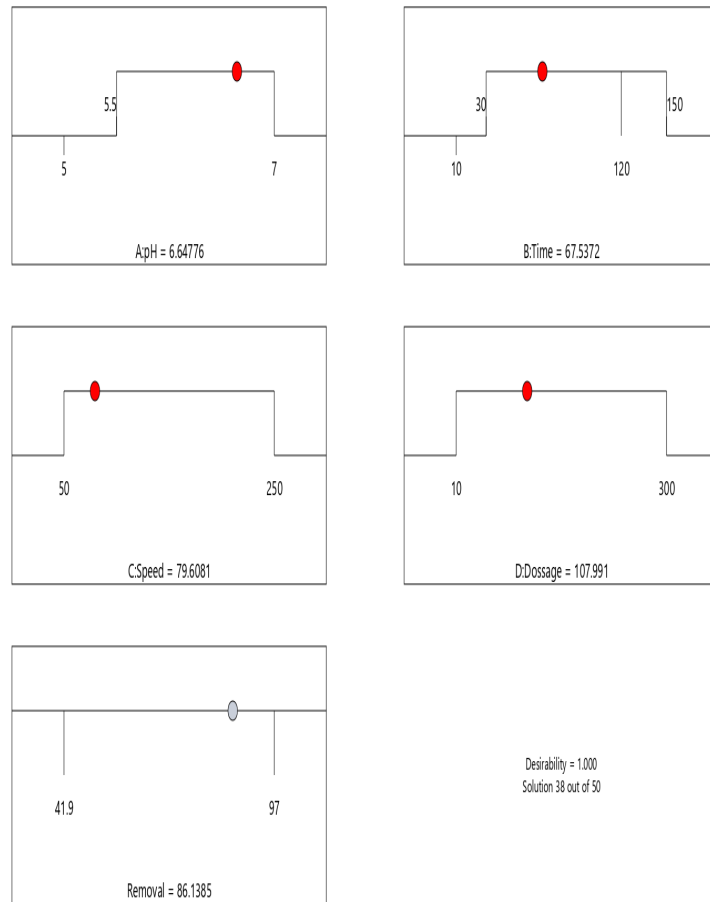


Fig. 12. Graphical Parameters optimization for 2-NP elimination.

The Removal percentage and the Dispensity for the Optimum parameter for 2-NP are shown in Figure 13.

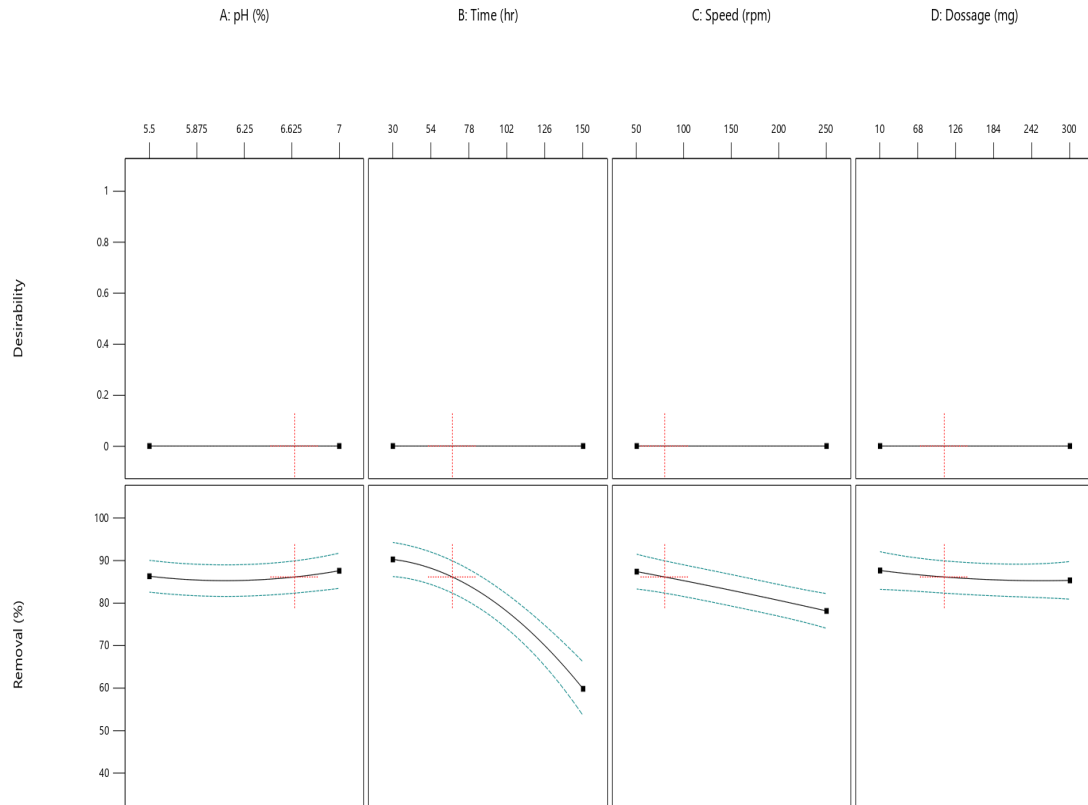


Fig. 13. Removal and the Dispersion for the Optimum parameter for 2-NP.

The Effect of adsorption time(hr) and the adsorbent dosage (mg) on the removal of 2-NP reprinted by response surface plot and Contour plot in Figure 14.

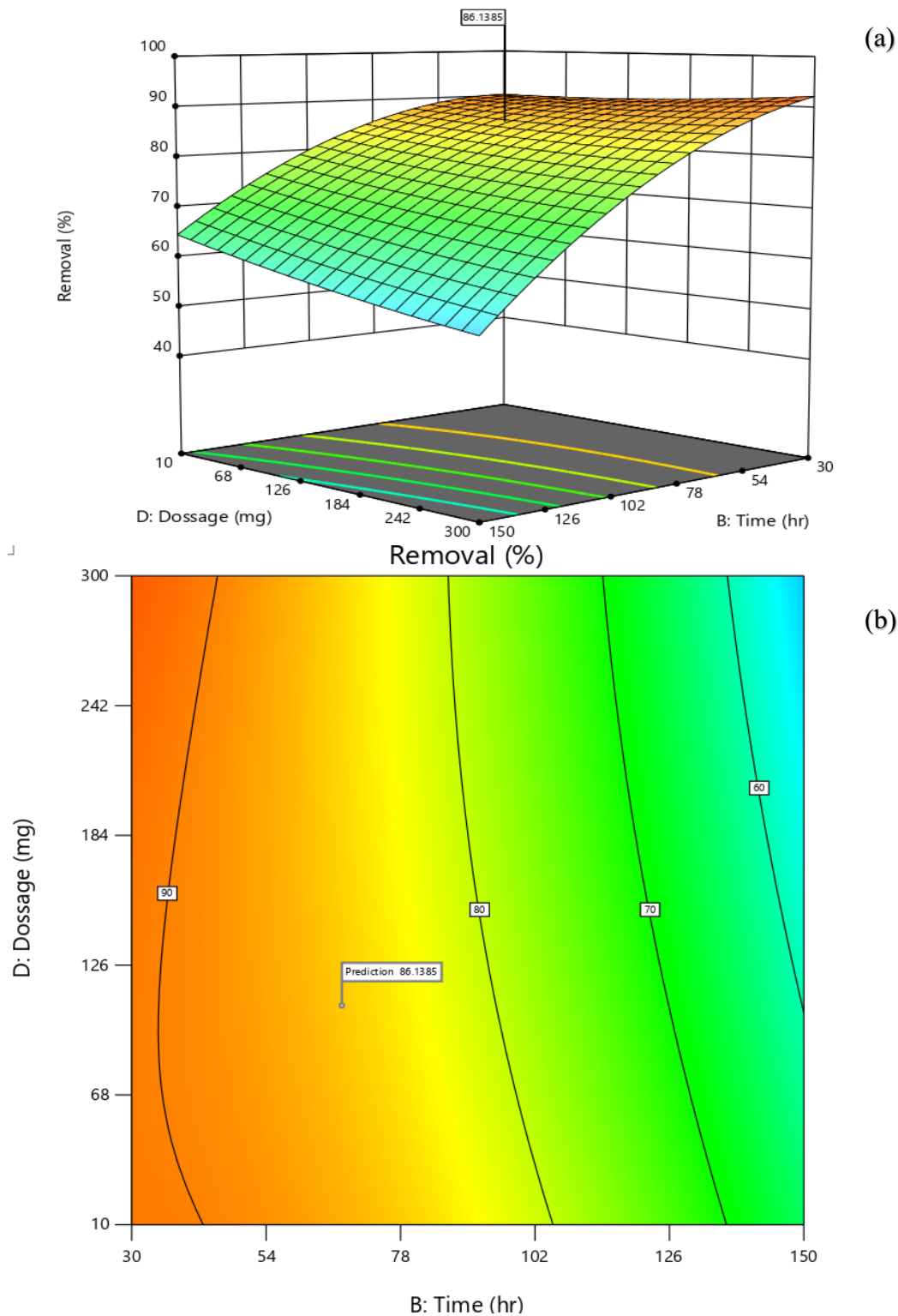


Fig. 14. Effect of adsorption time(hr) and the adsorbent dosage (mg) on the removal of 2- NP: :(a) Response surface plot and (b) Contour plot.

3.2 Adsorption of O-Nitrophenol

As shown in figure.15(a), the initial concentration of the 2-NP adsorption has an affection on the amount of 2-NP absorbed onto the nano adsorbent material, which decreases as the initial concentration increases as clearly seen in the graph. This is since a larger concentration of 2-NP leads to a lesser availability of adsorption sites on the adsorbent, which causes the observed effect. Furthermore, when beginning with a high concentration, mass transfer limitations may slow down the rate of adsorption. The adsorption of 2-NP was studied in a volumetric flask containing 100 ml of liquid at a concentration of 5 parts per million. By using the calibration curve, the concentrations of 2-NP could be determined both at the start and at the end of the experiment. Adsorption was evaluated by varying the adsorption parameters (obtained from RSM) in a solution at room temperature (298.15 K), with a pH of 6.6, an adsorption period of 68.0 minutes, 108 mg Dosage and a shaking speed of 80 rpm. This was done to assess the adsorption's efficiency. According to the findings, the adsorption was completed successfully. Table 8 summarizes the results, which include the total percentage of 2-NP eliminated, as well as the adsorption capacity of raw and activated CNFs and CNTs.

Table 8: The adsorption capacity of CNFs and CNTs for 2-NP

Adsorbent	Removal [%]	Q [mg/g]
CCNFs	18.49	0.6789
CCNFs/HCL	62.33	1.669
MWCNTs	52.66	1.50
MWCNTs/HCL	84.17	1.982

As shown in Fig. 15(b), the efficiency of removal of the activated nano adsorbent is better than in their raw state. The CNTs show an increase of about 30% in removal efficiency compared to the raw CNTs. Additionally, it is also observed that the treated CNFs enhance the removal efficiency even more than the raw CNFs. This indicates that the activation process, such as acid treatment, can significantly improve the adsorption capabilities of the nano carbon adsorbents by increasing their surface area and electrostatic interactions with the adsorbate molecules. The acid treatment improved the electrostatic interactions between the adsorbate molecules and the surface of the nano carbon adsorbents. The acidified environment can protonate the surface of the nano carbon adsorbents, creating a higher density of negative charges on the surface [39]. This can increase the electrostatic attraction between the positively charged 2-NP molecules and the negatively charged surface of the carbon nano adsorbents, leading to an increase in the amount of 2-NP absorbed onto the adsorbents. Additionally, acid treatment was found to increase the surface area of the adsorbents (as reported in Table 2) by breaking down its particles, providing more surface area for adsorption to occur. Therefore, acid treatment can favor the 2-NP adsorption process by increasing the electrostatic interactions and the surface area available for adsorption. The RSM approach was successful in optimizing removal efficiency, as demonstrated by the predicted removal rate of 2-NP being 87.13%, compared to the actual experimental rate of 84.17%. This indicates that the removal was effectively improved.

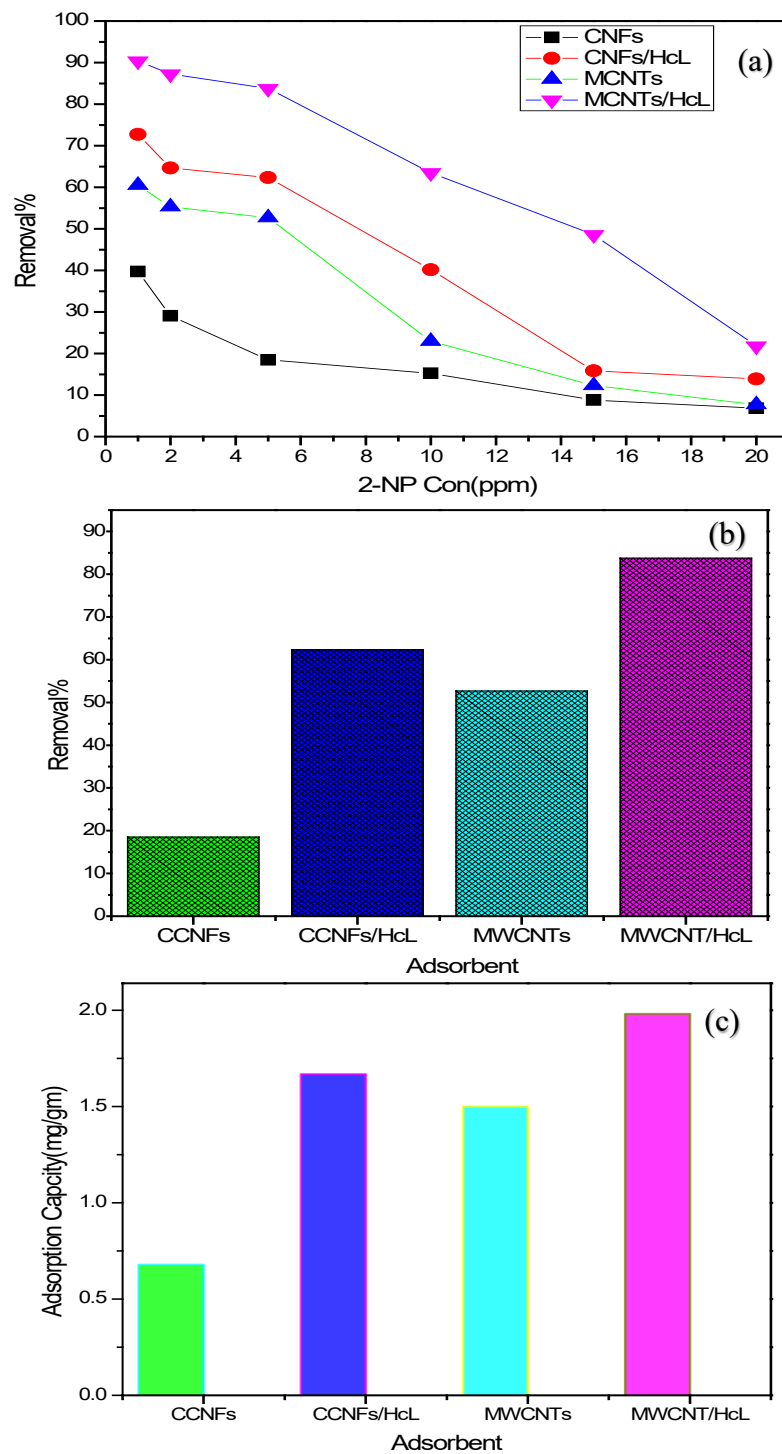


Fig. 15. Adsorption of 2-NP(5ppm) by raw and activated adsorbents at room temperature 298.15 K, pH 6.6, Adsorption time: 68 minutes, Nano adsorbent dosage: 108 mg and shaking speed 80rpm; (a) Effect of initial concentrations on the removal efficiency (b) The maximum removal rate after reaching adsorption equilibrium; (c) Comparison of adsorption capacities of the raw and treated CCNFs and MCNTs adsorbents.

4. CONCLUSION

This study found that acid treatment enhances the ability of nanomaterials to absorb pollutants in wastewater treatment. The research showed that acid-treated multi-walled carbon nanotubes (MCNTs) were more effective at reducing 2-nitrophenol levels in water compared to acid-treated carbon nanofibers (CNFs). Analysis of the SEM images, FT-IR spectra, BET, and 2-NP removal percentages revealed that acid treatment effectively removed impurities from the surface of raw CNTs and CNFs, resulting in a nano-porous structure without damaging the overall structure of the CNT fiber film. The acid modification was found to be more effective at opening the tips of the tubes on the surface of MCNTs than the tips of fibers on the surface of CNFs. The perfect parameters for extracting 2-NP and increasing adsorption capacity predicted by RSM provided a removal efficiency of 87.14, while the achieved removal from experimental results produced 84.17%. Overall, this research highlights the potential of using nanotubes and nanofibers in various pollution treatment applications and opens the door for further research to develop more efficient adsorbents.

ACKNOWLEDGMENTS

The authors would like to thank the Centre for Hydrogen and Energy Storage and the Core Research Facilities Center at KFUPM for providing access to FTIR and XRD analyses, as well as TEM and SEM screening.

REFERENCES

- [1] Calace N, Nardi E, Petronio BM & Pietroletti M. (2002) Adsorption of phenols by papermill sludges. *Environmental Pollution*,118(3):315-319.
- [2] Ali Amer Yahya, Khalid T. Rashid, et al. (2021) Removal of 4-Nitrophenol from Aqueous Solution by Using Polyphenyl Sulfone-Based Blend Membranes: Characterization and Performance. *J. Membranes*,11(3):171.
- [3] Akash Balakrishnan, Ghanghor Jayant Gaware, Mahendra Chinthala. (2023) Heterojunction photocatalysts for the removal of nitrophenol: A systematic review. *Chemosphere*, 310:136853.
- [4] Rida Fatima, Muhammad N. Afridi, Vanish Kumar, Jechan Lee, Imran Ali, Ki-Hyan Kim, Jong-Oh Kim. (2019) Photocatalytic degradation performance of various types of modified TiO₂ against nitrophenols in aqueous systems. *J Clean Prod*, 231:899-912.
- [5] Abdollahi M, Mohammadirad A. (2014) Nitrophenol, 4. In: Wexler P, ed. *Encyclopedia of Toxicology (Third Edition)*. Oxford: Academic Press, 575-577.
- [6] Pawan K. Gupta. (2017) Chapter 37- Herbicides and Fungicides. *Reproductive and Developmental Toxicology*,2,657-679.
- [7] Arora, P.K., Srivastava, A and Singh, V.P. (2014) Bacterial degradation of nitrophenols and their derivatives. *J Hazard Mater*, 266, 42–59.

- [8] A. Gómez-Avilés, L. Sellaoui, M. Badawi, A. Bonilla-Petriciolet, J. Bedia. (2021) Simultaneous adsorption of acetaminophen, diclofenac, and tetracycline by organo-sepiolite: experiments and statistical physics modelling. *Chem Eng J*,404, 126601.
- [9] Lotfi Sellaoui, Luis F.O. Silva, et al. (2021) Adsorption of ketoprofen and 2-nitrophenol on activated carbon prepared from winery wastes: A combined experimental and theoretical study. *Journal of Molecular Liquids*,333,115906.
- [10] Y. Dehmani, L. Sellaoui, Y. Alghamdi, J. Lainé, M. Badawi, A. Amhoud, et al. (2020) Kinetic, thermodynamic and mechanism study of the adsorption of phenol on Moroccan clay. *J Mol Liq*,312,113383.
- [11] Z. Li, A. Gómez-Avilés, L. Sellaoui, J. Bedia, A. Bonilla-Petriciolet, C. Belver. (2019) Adsorption of ibuprofen on organo-sepiolite and on zeolite/sepiolite heterostructure: synthesis, characterization, and statistical physics modeling. *Chem Eng J*, 371:868-875.
- [12] L. Sellaoui, Z. Li, M. Badawi, G.L. Dotto, A. Bonilla-Petriciolet, Z. Chen. (2020) Origin of the outstanding performance of Zn Al and Mg Fe layered double hydroxides in the adsorption of 2-nitrophenol: A statistical physics assessment *J Mol Liq*, 314,113572.
- [13] S. Nouri, F. Haghseresht, G.Q.M. Lu. (2002) Comparison of adsorption capacity of p-cresol & p-nitrophenol by activated carbon in single and double solute. *J Adsorption*, 8:215-223.
- [14] Yazidi, A., Sellaoui, L., Dotto, G. L., Bonilla-Petriciolet, A., Fröhlich, A. C., & Lamine, A. B. (2019) Monolayer and multilayer adsorption of pharmaceuticals on activated carbon: Application of advanced statistical physics models. *Journal of Molecular Liquids*,283,276-286.
- [15] Fu, F.,& Wang, Q. (2011) Removal of heavy metal ions from wastewaters: A review. *J Environ Manag*, 92(3): 407–418.
- [16] Lu, F.,& Astruc, D. (2018) Nanomaterials for removal of toxic elements from water. *Coord Chem Rev*,356, 147–164.
- [17] Agarwal, M., & Singh, K. (2017) Heavy metal removal from wastewater using various adsorbents: A review. *J Water Reuse Desalin*,7(4):387–419.
- [18] Alguacil, F.J., Lopez, F.A.& Garcia-Diaz, I. (2016) Extracting metals from aqueous solutions using Ti-based nanostructures: A review. *Desalin Water Treat*, 57(37):17603-17615.
- [19] Alguacil, F.J., Lopez, F.A.,O. Rodriguez, S.Martinez-Ramirez, S.& Garcia-Diaz, I. (2016) Sorption of indium (III) onto carbon nanotubes. *Ecotoxicol Environ Saf*,130,81-86.
- [20] Salam, M.A., Makki, M.S.I., Abdelaal,M.Y. (2011) Preparation and characterization of multi-walled carbon nanotubes/chitosan nanocomposite and its application for removal of heavy metals from aqueous solution. *J Alloy Compd*, 509(5):2582–2587.
- [21] Baby, R., Hussein, M. Z., Abdullah, A. H., & Zainal, Z. (2022) Nanomaterials for the treatment of heavy metal contaminated water. *Polymers*, 14(3), 583.
- [22] Sumio Iijima. (1991) Helical microtubules of graphitic carbon. *Nature*,354(6348): 56–58.
- [23] Popov, V.N. (2004) Carbon nanotubes: properties and application. *Mater Sci Eng: R: Reports*, 43(3):61–102.
- [24] Endo, M., Kroto, H.W. (1992) Formation of carbon nanofibers. *The Journal of Physical Chemistry*, 96(17):6941-6944.
- [25] Ebbesen,T.W., &Ajayan,P.M. (1992) Large scale synthesis of carbon nanotubes. *Nature*, 358(6383): 220–222.

- [26] Kondratyuk, P., & Yates Jr, J. T. (2007) Molecular views of physical adsorption inside and outside of single-wall carbon nanotubes. *Acc Chem Res*, 40(10): 995–1004.
- [27] Chatterjee, A., & Deopura, B. L. (2002) Carbon nanotubes and nanofiber: an overview. *Fibers and Polymers*, 3(4):134–139.
- [28] Inagaki, M., & Radovic, L. R. (2002) Nanocarbons. *Carbon*, 12(40) :2279–2282.
- [29] Subhani, T., Shaffer, M. S. & Boccaccini, A. R. (2013) Carbon Nanotube (CNT) reinforced glass and glass-ceramic matrix composites. In *Ceramic Nanocomposites*, 208-256. Wood head publishing.
- [30] Pierson, H. O. (1999) *Handbook of Chemical Vapor Deposition: Principles, Technology and Applications*. William Andrew, New York, NY, USA, 2nd edition.
- [31] Park, C., Engel, E. S., Crowe, A., Gilbert, T. R. & Rodriguez, N. M. (2000) Use of carbon nanofibers in the removal of organic solvents from water. *Langmuir*, 16(21):8050–8056.
- [32] Oh, G. Y., Ju, Y. W., Kim, M. Y., Jung, H. R., Kim, H. J., Lee, W. J. (2008) Adsorption of toluene on carbon nanofibers prepared by electrospinning. *Sci Total Environ*, 393(2-3):341–347.
- [33] Lee, S. (2010) Application of activated carbon fiber (ACF) for arsenic removal in aqueous solution. *Korean J Chem Eng*, 27:110–115.
- [34] Chakraborty, A., Deva A. D. Sharma, A. & Verma, N. (2011) Adsorbents based on carbon microfibers and carbon nanofibers for the removal of Phenol and lead from water. *J Colloid Interface Sci*, 359(1):228–239.
- [35] Li-Y. H., Ding, J., Luan, Z., Di, Z., Zhu, Y., Xu, C., & Wei, B. (2003) Competitive adsorption of Pb^{+2} , Cu^{+2} and Cd^{+2} ions from aqueous solution by carbon nanotubes. *Carbon*, 41(14):2787-2792.
- [36] Deng, X., Lu, L., H., & Luo, F. (2010) The adsorption properties of Pb (II) and Cr (II) on functionalized graphene prepared by electrolysis method. *J Hazard Mater*, 183(1-3):923-930.
- [37] Wang, S., Ng, C. W., Wang, W., Li, Q., & Hao, Z. (2012) Synergistic and competitive adsorption of organic dyes on multiwalled carbon nanotubes. *Chemical Engineering Journal*, 197,34-40.
- [38] Brunauer, S., Emmett, P. H., & Teller, E. (1938). Adsorption of gases in multimolecular layers. *Journal of the American chemical society*, 60(2):309-319.
- [39] Hoon Hyung & Jae-Hong Kim. (2008) Natural Organic Matter Adsorption to Multi-Walled Carbon Nanotubes: Effect of NOM Characteristics and Water Quality Parameters. *Environ Sci Technol*, 42 (12):4416–4421.
- [40] G Horváth & K Kawazoe. (1983) Method for the calculation of effective pore size distribution in molecular sieve carbon. *Journal of Chemical Engineering of Japan*, 16(6), 470-475.
- [41] FTIR Functional Group Table Available: <http://instanano.Com/all/characterization/fir/fir-functional-group-search>.
- [42] Lu, Y., Liu, Z., You, S. W., McLoughlin, L., Bridgers, B., Hayes, S., & Wujcik, E. K. (2020) Electrospun carbon/iron nanofibers: The catalytic effects of iron and application in Cr (VI) removal. *Carbon*, 166 :227-244.
- [43] R. L. Vander Wal, T. M. Tichich, & V. E. Curtis. (2000) Directed synthesis of metal-catalyzed carbon nanofibers and graphite encapsulated metal nanoparticles. *The Journal of Physical Chemistry B*, 104 (49) :11606–11611.
- [44] P. Tribolet & L. Kiwi-Minsker. (2005) Carbon nanofibers grown on metallic filters as novel catalytic materials. *Catalysis Today*, 102: 15–22.

- [45] Aoki, K., Yamamoto, T., Furuta, H., Ikuno, T., Honda, S., Furuta, M., & Hirao. (2006) Low-temperature growth of carbon nanofiber by thermal chemical vapor deposition using CuNi catalyst. *Japanese Journal of Applied Physics*, 45 (6R):5329–5331.
- [46] Cruz-González, K., Torres-López, O., García-León, A., Guzmán-Mar, J. L., Reyes, L. H., Hernández-Ramírez, A., & Peralta-Hernández, J. M. (2010) Determination of optimum operating parameters for Acid Yellow 36 decolorization by electro-Fenton process using BDD cathode. *Chemical Engineering Journal*, 160(1):199-206.
- [47] Zabeti, M., Daud, W. M. A. W., & Aroua, M. K. (2009) Optimization of the activity of $\text{CaO}/\text{Al}_2\text{O}_3$ catalyst for biodiesel production using response surface methodology. *Applied Catalysis A: General*, 366(1):154-159.
- [48] Virkutyte, J., Rokhina, E., & Jegatheesan, V. (2010) Optimisation of Electro-Fenton denitrification of a model wastewater using a response surface methodology. *Bioresource technology*, 101(5): 1440-1446.
- [49] Gutiérrez, H., & De La Vara, R. (2008) *Análisis y diseño de experimentos*. México DF: McGraw-Hill Interamericana.
- [50] Serp, P., & Machado, B. (2015). *Nanostructured carbon materials for catalysis* (No. 23). Royal Society of Chemistry.